

Project Description

Tandem Proposal Within the DFG-SPP2171/1 Dynamic Wetting

DYNAMIC WETTING AND DEWETTING OF VISCOUS LIQUID DROPLETS/FILMS
ON VISCOELASTIC SUBSTRATES

RALF SEEMANN (SAARLAND UNIVERSITY), BARBARA WAGNER (WIAS)

1 State of the art and preliminary work

State of the art

In recent years, the interaction of liquid films and droplets well below the capillary length with elastic substrates has been receiving increasing attention [1]. Two aspects have been particularly intensively studied: The question of the shape of an equilibrium droplet and the contact angles at the three phase contact line where the solid-vapour, solid-liquid and liquid-vapour interfaces meet, and, second, the possibility and impact of the Shuttleworth effect [2].

In [3], the authors investigate the shape of the droplet (without the Shuttleworth effect) by minimising the elastic and capillary free energy and find that it is determined by three length scales, the ratio of surface tension to elastic modulus γ/E , the molecular size a and the size of the droplet R . The ratio between the first two length scales determines if the microscopic contact angles follow Young's law (as for a rigid solid) or Neumann's law (as for two liquids), while the ratio between the first and third determines the transition from Young to Neumann's law for the macroscopic contact angle. Recently, Hui and Jagota [4] suggested that even the correct approach to formulating the conditions for the contact angles for a droplet are still open for debate, that is, whether a variation approach through an energy balance should be used, or a mechanical balance of forces; the authors in fact argue that a combination of both is required.

The Shuttleworth effect is based on the observation that solid-fluid interfaces are potentially different from liquid-liquid interfaces, in that for the former, a strain dependence of the surface tension is possible [2]. Since then, the topic has been discussed controversially regarding both the existence of this effect and even the question how to include the Shuttleworth model into drop and film models on substrates is ongoing research. Xu et al. [5] observe that the angle θ_S at the triple contact-line between the solid-liquid and solid-vapour increases when the silicon gel substrate is stretched. In contrast, Schulman et al. [6] determine the angle θ_L between the solid-liquid and liquid-vapour interface in their experiment and observed it is largely independent of the strain for a range of elastomers, hence gives evidence against the present of a Shuttleworth effect. Snoeijer et al. [7] resolve this apparent paradox by studying a variationally derived model for the static droplet with the Shuttleworth equation for the surface equation. They conclude that, θ_L is not affected by the strain dependence of the surface energy, and hence is unsuitable to detect the Shuttleworth effect on soft elastic solids, while θ_S does change.

For very soft polymer substrates the elastic responses may become highly nonlinear, moreover the three-dimensional network of chemically or physically cross-linked polymer chains together with uncrosslinked polymer molecules may phase separate, e.g. at the dewetting ridge, leading in turn to deformations of the polymer network. This behaviour is of great interest for applications which use polymer gels in smart materials for example. However, many questions including at the modelling level are not yet understood but have been receiving increasing attention in the past years. Two properties make polymer gel substrates particularly interesting and will lead to new challenges and insight compared beyond what

we expect from the other material systems we are studying. One is that the softness of the material leads to strong elastic responses and nonlinear elasticity will manifest itself. Second, the heterogeneous nature of the material as a combination of solvent and network can vary locally in time and space, leading to the possibility of phase-separation type phenomena. Both are expected to occur most likely in the contact angle region that is so important for both the statics and dynamics of wetting and dewetting phenomena.

The equilibrium theory of gel goes back to the seminal papers by Flory et al. [8] they took up earlier work by Frenkel (cited therein) and developed it into a general theory. They propose a free energy with two competing contributions: One represents the contribution from the (rubberlike) elasticity and the other is the mixing free energy, which determines the affinity of the solvent and polymer molecules for each other. Diffusion of further polymer molecules into the network usually increases the degree of interaction, hence lowers the mixing energy, but also leads to more stretching. These contributions need to balance at equilibrium.

For kinetic models, linear poroelastic theory has been used [9, 10] but these are restricted to infinitesimal deformations and they typically neglect the interaction energy between the solvent and the polymer segments i.e. part of the mixing energy. These limitations can be overcome by combining the constitutive laws for the free energy of elastomeric gels with a theory for large-deformation poroelasticity [11–14]. These approaches differ regarding some of the details, for example, whether the motion of the solvent molecules within the network is by Fickian diffusion or is pressure-driven and follows Darcy’s law in a porous medium. In [13] Drozdov et al. use a thermodynamically motivated energy imbalance inequality argument by Gurtin [15] which was applied to gels by [14] and derive a kinetic law for the gel that naturally includes both contributions and relates the two mobility coefficients.

The mixing energy contribution that appears in the free energy of the Flory-Rehner formulations itself has two types of contributions, namely terms that reflect the effect of entropy and always enhance mixing and the interaction terms between the polymer segments and the solvent which can also promote separation. This indicates that the Flory-Rehner theory in principle allows for phase separation into regions of different compositions, but of course depends on the full free energy including the elastic terms. Phase separation is observed in experiments for example at the triple-phase contact line in soft adhesion experiments [16]. In dewetting experiments, the additional tension at the contact-line can also promote a separation of free polymer molecules from the cross-linked polymer network, which in turn can moderate the dissipation at the contact line and hence affect dewetting rates, for example, and should be captured in a model as a phase-separation phenomenon.

In contrast to the large body of existing theoretical work only limited activities were dedicated to explore the wetting and dewetting on elastic substrates experimentally. Most of them focused on static situations, either on solid particles sitting on an elastomeric surface [17–21] or on the deformation of an elastic substrate around the three phase contact line potentially including the "bottom" side of a sessile droplet [18, 22–24]. The latter experiments were typically conducted using macroscopic droplets imaged by confocal microscopy while meanwhile for some systems a satisfactory agreement between experimentally obtained three phase contact lines and theoretical results were obtained. Liquid droplets can also interact with gradients in elastic module and move along those gradients and finally form droplet pattern reflecting the underlying buried topography respectively patterns of locally varying elastic module [25]; this effect is referred to as durotaxis. The decaying of a "liquid step" using the leveling method [26] on top of an elastomer interface was imaged experimentally and the strain field in the elastomer substrate was determined theoretically yielding satisfactory agreement with experimentally determined shape and dynamic of the decaying step, however no liquid-elastomer-air three phase contact line is present in this system.

In the pioneering work of Shanahan and Carré [27] the authors demonstrated that in contrast to liquids sliding down inclined solid substrates, parts of the work is dissipated to deform the substrates when droplets slide down elastic substrate. This effect was termed the "viscoelastic breaking" and supported

previous predictions [28]. Shanahan and Carré [29] extended their experimental study and found that the radius of the optically observed dewetting holes grow linearly in time and the dewetting velocity increases also linearly with the Elastic modulus of the substrate; the latter was even supported by a simple theory.

Since then there were only few additional experiments conducted that consider the dynamics of droplets respectively the dynamics of three phase contact lines on elastomeric substrates. Droplets that are inflated through a needle was studied in [30] and the authors presented a scaling law, able to capture the main physical processes that control the transition from rapid inertial to slower viscoelastic spreading of low-viscosity drops on elastomeric polydimethylsiloxane (PDMS) substrates with shear moduli ranging from about 20 to 700 kPa. In [31] elastic rods were pulled out of a liquid reservoir in a setup similar to dip coating. In this work it is concluded that the details of elastocapillary interactions cannot be captured by macroscopic thermodynamic arguments and requires microscopic modeling. An influence of the "viscoelastic breaking" was also observed in [32] where the drop impact and spreading or bouncing on elastomeric substrates was explored. The advancing contact angle of a sessile liquid drop being inflated on a very soft ($\lesssim 1$ kPa) gel surface was studied e.g. in [33]. The authors observed velocity dependent contact line motion with a pronounced stick-slip motion at intermediate velocity regimes that depend on the rheological properties on the gel. A year later, the same group studied also the velocity dependent receding contact line motion on the same type of gel surface using a tip coating geometry [34] and obtained similar results.

High resolution X-ray microscopy with a pixel resolution of about 50 nm was applied in [35] to image the dynamic shape of a three-phase contact line. Based on the obtained results, the authors concluded that "the slow and linear growth of the ridges with the invariant contact angles suggests that the ridge growth is caused by a viscous flow in the soft solid, similar to that in a very viscous liquid". And it is claimed that "viscoelastic deformation of the ridge has been also observed even on elastomers" and "further studies are required to correlate the ridge growth and the plastic deformation".

Preliminary work

The applicants have ample experience studying the dewetting of polymer thin films with particular focus on the break up mechanism e.g. [36–38], the shape of the emerging dewetting rim profile and the energy dissipation process in the liquid and at the solid-liquid interface (slip) [39–41]. These studies were recently extended to liquid dewetting from another liquid substrate where additional work in the liquid substrate is needed to move the dewetting rim [42–44]. Also a strategy was developed to study nanoscopic droplets, contact line motion and three-dimensional rim profiles of thin liquid polystyrene films dewetting on rubber elastic substrates of different elastic moduli [45].

Experimental studies For these preliminary dewetting results elastomeric substrates about $6 \mu\text{m}$ thick layers of SYLGARD®184 (SG184) and SYLGARD®186 (SG186) (Dow Corning) were prepared on silicon substrates. The elastic moduli of SYLGARD depend on external factors such as the curing procedure. For the preparation protocol applied here, we determined the elastic module to range between 1.5 MPa (for SG186) and 5.0 MPa (for SG184). To prepare substrates with elasticities in-between pure SG184 and SG186, we prepared mixtures of SG184 and SG186 with weight ratios 1:2, 1:3 and 1:6.

Figure 1 shows the dewetting of a thin polystyrene (PS) films from elastomeric substrates. The dewetting is faster on the stiffer SG184 and gradually slows down as the rubber gets softer. For all elasticities dewetting is faster for small holes and slows down as the width of the dewetting rim grows. As the contact angle of $\theta_e = 62 \pm 1^\circ$ is not affected by the elastic module, this result already implies that the energy is not just dissipated at the three phase contact line but also somewhere at the elastomer-liquid interface or in the elastomer - be it slip friction or "viscoelastic breaking" as suggested by [28].

The dependence of dewetting rates from elastic module is qualitatively in good agreement with the

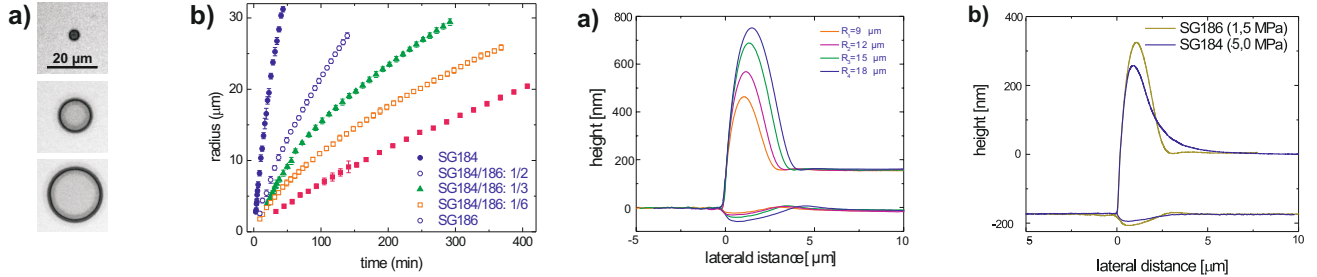


Figure 1: Dewetting of a 150 nm thick PS(17.4k) film at 120°C. Left: a) Optical microscopy images. b) Dewetting rates on substrates of different elasticities. SG184(k)-SG186(n) stands for a substrate prepared from k parts of SG184 mixed with n parts of SG186 (w/w). Right: a) Cross-sections of AFM scans of a dewetting rim around a hole with radii of 9 μm , 12 μm , 15 μm , 18 μm . b) Comparison of rim profiles on SG186 and SG184.

results of Carré and Shanahan [46], who measured the velocity of a liquid droplet running down an inclined elastomeric plane. The emerging wetting ridge and exterior substrate profile has already been verified experimentally by Carré et al. [47], by an interferometric technique. According to their model, the vertical displacement $h(x)$ of the substrate as a function of the distance from the TPCL, is:

$$h(x) = \frac{\sigma_{LV} \sin \theta_e (1 + \nu)}{\pi E} \ln \left(\frac{d}{x} \right), \quad x > \epsilon \quad (1)$$

where ν is the Poisson's ratio of the elastic substrate, which is considered incompressible, thus $\nu = 0.5$, E is the elastic modulus, d is the horizontal distance between the TPCL and the undisturbed substrate and ϵ is a length scale about the line of application inside which the material is plastically deformed by the surface tension force, whereas outside this region, linear elasticity is assumed to be valid. Comparing the shape of the substrate in the vicinity of the three phase contact line found in our experiments with the calculated one given by eq. 1, we observe a good agreement for SG184, but a remarkable deviation for the softer substrates fig. (2b).

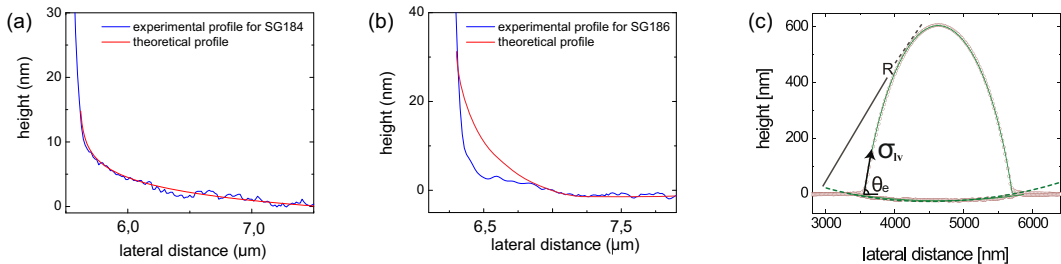


Figure 2: a,b) Experimental (blue curves) and theoretical (red curves) profiles of the substrate deformation in the vicinity of the three-phase contact line for thin a) SG184 and b) SG186 substrate. c) 3D profile of droplet sitting on SG184 substrate obtained by combining AFM scans of the top and bottom side of the same droplet. The green curves are circular fits. θ_e is the contact angle, σ_{lv} is the liquid-air surface tension and R the radius of curvature of the "indentation".

The shape of the PS-elastomer interface that is frozen into the glassy PS can be obtained by lifting off the PS and imaging its "bottom side". Details of the lift off technique will be presented in the work program. From the 3d droplet shape the elastic module E of the elastomer substrate can be estimated by applying a Hertzian model and assuming the indentation to have the shape of a spherical cap that is formed by a rigid indenter of radius R . However, this assumption is only fulfilled for very small droplets as the bottom shape of larger droplets are flattened. The "indentation force" is applied by the vertical component of the surface tension σ_{LV} along the perimeter of the droplet.

Inspecting the 3d-rim shapes during dewetting fig. 1, we can distinguish several characteristic features, that adapt with elastic modulus and during hole growth. We e.g. observe a "depletion" zone at the dry side of the dewetting rim for the soft SG186 substrate, which indicates that some of the substrate material is dragged tangentially with the dewetting liquid. A quantitative comparison to theoretical predictions should clarify the various contributions, potential strain dependent contact angles, and energy dissipation mechanisms that lead to the observed dewetting scenarios.

Theoretical studies Our studies concerned mainly problems with two-layer systems, where a thin liquid film on the thickness scale of about a 100 nm, retracts from a liquid substrate from about 100 nm to several μm . Theoretical models were developed in Jachalski et al. [48, 49], that take account of intermolecular forces, interfacial *apparent slip* as well as nonlinear viscoelastic effects. Mathematical analysis of the stationary and dynamic problems as well as numerical methods for the associated thin-film that could be derived as well as the underlying free boundary problem for the Stokes equations were carried out. For the model of the two-layer system we considered in each layer the Cauchy momentum equations At the solid-liquid interface impermeability is assumed and an *apparent slip* which is modelled via a Navier-slip condition with an effective effective slip-length b . At the liquid-liquid interface, a kinematic condition balances the normal component of the velocity of liquid at the interface with the velocity of the interface itself. Capillary forces are compensated by the jump of the stress tensors times unit normal vector and also by intermolecular forces, leading to the tangential and normal stress condition together with slip and impermeability condition at this surface. The upper (liquid-air) free surface evolves according to a kinematic condition, together with the tangential and normal stress conditions, [48] for a detailed formulation.

At these scales the dewetting dynamics is drive by intermolecular forces given by a intermolecular potential that consists of two competing terms, which represent long-range interaction, giving rise to the the disjoining pressure from the van-der-Waals potential that drives the dewetting, and short-range, that stabilises the height to a value h_* for which the potential has a minimum $\phi_* < 0$.

In [50] stationary solutions where obtained and in the limit $h_* \rightarrow 0$ the three-phase contact angle (Neumann triangle) was derived using matched asymptotic expansions. Values for surface tension and the equilibrium contact angles were derived by comparing experimentally obtained equilibrium morphologies of the PS/PMMA system with exact analytical solutions.

We first considered the evolution of liquid PS drop shapes on liquid PMMA substrate into equilibrium. Numerical results were obtained by solving the associated thin-film equations for the two-layer films of Newtonian liquids. Interestingly, our parameter studies revealed that the transient drop shapes having identical volume synchronise, with a distinct morphology of the liquid-liquid interface, after a certain dewetting time and are independent on the particular starting or initial configuration. This synchronisation occurs both for different initial film heights as well as for non-rotational symmetric initial PS patches, and remain in this quasi-stationary state before equilibrium (lense shaped morphology) is reached. Moreover, they undergo the same morphological stages into equilibrium. Comparing experimentally measured and theoretically computed interface profiles during dewetting of Newtonian liquid from a Newonian liquid susbtrate with order one viscosity ratios and comparable thickness of the layers showed excellent agreement of both the characteristic shapes of the liquid-air/substrate-air interfaces measured by in-situ AFM, see [44] for this comparison.

Most interesting is that right next to the contact line, the liquid-liquid interface extends deep into the substrate and generates a trench which generates additional resistance against the dewetting motion. The size of this trench depends only weakly on the size of the growing dewetting rim, i.e., the dewetting distance. For small dewetting distances, the dewetting rates suggest a linear behaviour for all thickness ratios in agreement with the results by Lambooy et al.[51]. For fixed substrate film thickness \bar{h}_s , the dewetting rates are larger for liquid layers thinner than the substrate, $\bar{h}_\ell < \bar{h}_s$, and smaller for thicker

liquid layers, $\bar{h}_\ell > \bar{h}_s$. But, a close inspection of the seemingly constant dewetting rates indicated that the dewetting velocity slowly decreases over time. The dependence of the dewetting rates was then established from simulation for physical dewetting times, which are not accessible experimentally together with further results for other film thickness ratios.

To shed some light on the transient dewetting rates we discussed the possible physical dissipation mechanisms. We had previously observed in [41] that for rigid substrates the dissipation is predominantly localized near the contact line and in the bulk domain. The contact line area does not scale with volume, whereas the gradients in the dissipation cancel the growth of the cross-sectional area, thereby both leading to a linear dewetting law, however with logarithmic corrections [52]. Similarly, the power-law dewetting rates on liquid substrates predicted by Brochard et al. [53] rely on this assumptions that the dissipation is generated in only one such localized zone together with a nearly self-similar growth of rim shapes. However, these assumptions fail in the considered situation of liquid-liquid dewetting since dissipation is clearly not generated in one single zone but accumulates in the substrate, in the liquid and near contact lines on a similar order of magnitude. This explains why in our setting the liquid-liquid dewetting process is not in a regime dominated by a specific dissipation mechanism that would admit a simplification to a power-law rate, and thereby challenges the applicability of the theoretical results by Joanny[54] and Bochar-Wyart et al.[53] to experimental systems considered by the applicants. The weak scaling of the dissipation in the long-time limit theoretically explains the nearly linear dewetting rate [44], that was observed experimentally [51].

A very interesting theoretical study revealed that there are different asymptotic regimes in terms of the viscosity ratio of the two layers, which controls the morphology and dynamics of the system. In particular, when considering the regime of small viscosity ratio, by assuming $\mu := \frac{\mu_1}{\mu_2} \varepsilon^{-2} = O(1)$, [48] and keeping the ratio of the surface tensions $\sigma := \sigma_1/\sigma_2 = O(1)$, it was possible to obtain a closed form system of equations for h_1 , h , S and u_2 .

$$\partial_t h = -\partial_x(h u_2), \quad (2)$$

$$\partial_t h_1 = \frac{1}{12\mu} \partial_x (h_1^3 \partial_x p_1) - \frac{1}{2} \partial_x (h_1 u_2), \quad (3)$$

$$0 = -\frac{1}{2} h_1 \partial_x p_1 - h \partial_x p_2 + 4 \partial_x (h S) - \frac{\mu}{h_1} u_2, \quad (4)$$

$$0 = (1 + \lambda_{21} \partial_t + \lambda_{21} u_2 \partial_x) S - (1 + \lambda_{22} \partial_t + \lambda_{22} u_2 \partial_x) \partial_x u_2. \quad (5)$$

where $p_1 = -(\sigma + 1) \partial_{xx} h_1 - \partial_{xx} h$ and $p_2 = -\partial_{xx} h_1 - \partial_{xx} h + \phi'(h)$ where $(1 + \lambda_{21} \partial_t + \lambda_{21} u_2 \partial_x) S = (1 + \lambda_{22} \partial_t + \lambda_{22} u_2 \partial_x) \partial_x u_2$. This model is the first model that incorporates the full nonlinear corotational Jeffrey's model into a thin-film theory and offers the possibility to analyse as well as numerically study the nonlinear behaviour and long-time morphological evolution of the dewetting liquid-liquid system. In order

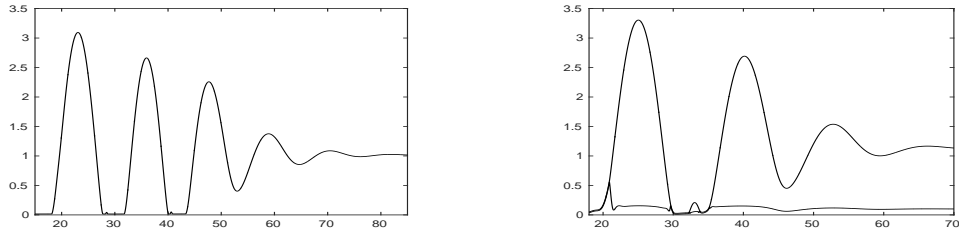


Figure 3: The strong-slip, viscoelastic model on a solid substrate, morphologies for large λ_1 (left). The small viscosity ratio, viscoelastic model (2), morphologies for large λ_1 (right)

to distinguish the impact of the viscoelastic rheology from the influence of a deformable liquid substrate

on the morphology of a dewetting film after rupture, we performed parameter studies for different initial stresses S , based on our previous models [55–57]. Apart from the shape of the rim, which attains the form of a parabola, the dewetting rate of the contact line is significantly slower in the viscoelastic case and it quickly pinches off, forming a new contact line, leading to a series of droplets. Moreover, for certain imposed initial stresses, also smaller secondary droplets pinch off just before the new contact line forms. For the corresponding situation for the two-layer model, i.e. we considered above model in the limit of a small viscosity ratio and a small initial thickness of the liquid substrate we observed qualitatively the same trends as the single layer problem. Differences are for example in the size of the droplets compared to the case of an solid substrate, in particular, the secondary droplets, which are larger see fig. 3 for the comparison. An intriguing morphology for large λ_{12} shows pinch off of the tail of the rim and a structure reminiscent to the “beads on a string” structure observed before in viscoelastic (Oldroyd-B) strings.

Our parameter study in [48] on the impact of the viscosity ratio of the two layers showed that in the Newtonian case the corresponding thin-film model for small viscosity ratios reduces to a model similar in structure to the so-called strong-slip model for the one layer situation. In particular, the well-known transition [41] from oscillatory to monotone decay of the rim tail for increasing slip lengths can also be observed for the two-layer, in this case for decreasing viscosity ratio. Similarly, as done in [52] one can capture this transition using a linear stability analysis about the undisturbed upper layer.

Linear stability analysis shows that a high-order (up to 8th order) polynomial equation for the growth rate σ is obtained was solved numerically for σ . A rather complex scenario arises, where dispersion curves

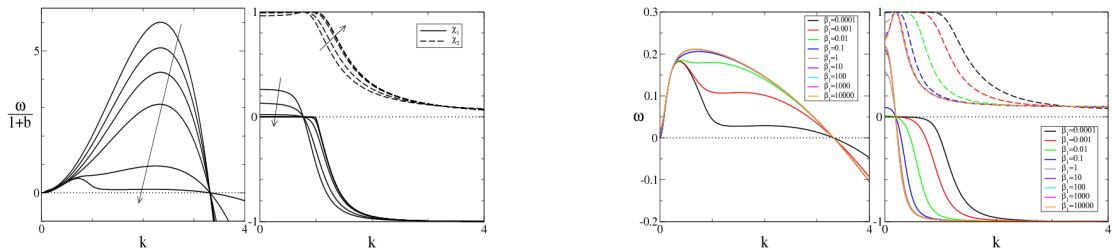


Figure 4: For $h_1 = 10$: Dispersion relations and components of the perturbation vector at both interfaces. For weak-slip with slip length $b = 0, \dots, 10^4$ (left, rescaled by $1+b$). Arrows point to increasing b . For the strong-slip model for $\beta = 10^{-4}, \dots, 10^4$ (right).

show transitions from dominant long-wave zig-zag modes to shorter wave varicose modes, depending on the relative thicknesses, viscosities, surface tensions of the layers. What is most interesting is that the presence of *apparent slip* or similarly the small viscosity ratio can completely change the transition threshold and the wavelengths of the unstable modes, as seen in for example in fig. 4, and hence needs to be accounted for when interpreting experimental results. As an example we show two dispersion relations that demonstrate the impact of slip (from weak to strong) on the spinodal wavelength.

1.1 Project-related publications [37, 40, 41, 43–45, 49, 56, 58, 59]

1.1.1 Articles published by outlets with scientific quality assurance, book publications, and works accepted for publication but not yet published

1.1.2 Patents NONE

2 Objectives and work programme

2.1 Anticipated total duration of the project 36 months, Oct. 2019 - Sept. 2021

2.2 Objectives

We aim at understanding the deformation of an elastomeric substrate that is caused by a liquid dewetting from it and the underlying energy dissipation mechanisms that influence the dewetting dynamics and rim shape. This shall be done as function of thickness and rheological properties of the substrate, and thickness and viscosity of the liquid film. For a quantitative comparison with theoretical predictions it is further needed to experimentally determine all relevant system parameters like contact angle, elastic module of the substrate and liquid viscosity sufficiently precisely.

Through detailed experimental-theoretical comparisons we aim to address the questions on the impact of strain-dependent surface energies on wetting and other elastocapillary phenomena. What governs the dynamic elastocapillary problem?

The typical experimental setup shall consist of a thin elastomer film supported by a solid silicon wafer. We intend to mainly use cross-linked Polydimethylsiloxane (PDMS) for these studies. Some physical and chemical attributes that make PDMS a suited material for our studies are: the big range of elasticities in which it can be found, its low glass transition temperature ($T_g = -125^\circ\text{C}$) and the virtually constant value of the elastic modulus versus frequency. The PDMS employed in our study will be prepared from commercially available silicon rubber/gel kits as will be detailed below.

2.3 Work programme incl. proposed research methods

WP E1: Optimize Preparation of Elastomer Systems (9 month) The dewetting of short chained polystyrene (PS) films on rubber elastic Sylgard 184 ($E \approx 5 \text{ MPa}$) and Sylgard 186 ($E \approx 1.5 \text{ MPa}$) substrates revealed a strong dependence of the dewetting velocity on the elastic module of the substrate, cf. fig. 1. However, a remarkable deformation of the liquid-rubber interface was only observed for the softer SG186 substrates [45]. Based on these preliminary results the desired range of elastic module starts at around 2 MPa, i.e. the elastic module of fully cross linked SG186 and reaches down to about 3 kPa, i.e. down to the elastic module of hydrogels. A particular challenge is the ability to prepare thin films of homogeneous and variable thickness from these materials on top of smooth and cleaned silicon substrates. Thin films are needed to guarantee a sufficient thermal conductivity, i.e. that the temperature of the hot plate can be assumed to be the same as the temperature of the sample surface, and second, the effect of elastic film thickness will be used as a control parameter. To achieve micrometer or sub-micrometer thin films of PDMS, the highly viscous PDMS mixtures shall be diluted with toluene to facilitate thin film preparation by spin coating. In the dilution ratios tested so far this protocol does not affect the rheological properties of the final PDMS film, as toluene evaporates completely during degassing and spin-coating. However, for other polymer mixtures or more extreme dilutions care has to be taken that there is no demixing during the spin coating leading to different rheological properties or non-curable mixtures. Curing of the PDMS shall be done in a protective atmosphere (N_2) to avoid different cross linking ratios at the interface and a "sticky" interface. Surface characterization and film thickness measurements of the prepared substrates shall be done by Atomic Force Microscopy (AFM) and potentially by ellipsometry in case of sub-micrometric films.

To achieve thin films of different elastic module, we will explore different commercially available silicon elastomers and gels. A typically used strategy in literature to obtain softer elastomers is to mix the two component elastomer kit SG184 in a ratio that deviates from the 10:1 ratio of based to curing agent as specified from the manufacturer e.g. [26]. However, besides a reduced elastic module down to about 50 kPa for a mixing ration of 40:1 [60] this strategy will lead to a reduced cross linking ratio and potentially to a sticky elastomer-air interface. As we plan to explore the dewetting process on larger scales by optical microscopy but also on smaller scales by in-situ AFM it will be important that the elastomer-air interface is not too sticky and allows for AFM imaging with acceptable risk of tip contamination. Moreover, non-complete cross-linking always has the risk of further cross linking and a changing elastic module during a dewetting temperature at elevated temperature.

Thus as an alternative we will rather use commercial products for the fabrication of elastomer substrates, which are available from Dow Corning, Momentive or Quantum Silicone (E.g. CY 52-276 A/B (Dow Corning) E \approx 3 kPa, DowsilTM SE 1740 (Dow Corning) durometer 35 (Shore 00)). Besides the exact mechanical properties it will be important to test that smooth films can be prepared of the respective elastomer material. We will also test special (e.g. fluorinated) elastomer kits that might provide different wettability with PS as a wetting liquid. As the rheological properties of thin films might deviate from bulk properties they will be determined using an existing Mars 2 shear rheometer and using the deformations caused by small droplets sitting in semi-infinite elastomer films as mentioned in the preliminary work.

To select suitable elastomer materials, optimize substrate preparations and determine rheological properties we estimate a duration of 9 month.

WP E2: Optimize and Bench Mark Lift Off Technique (9 month) Once the desired elastomer materials and preparation protocols are found, we will prepare glassy polystyrene (PS) films on top. This shall be done by spin-coating PS from a toluene onto a freshly cleaved mica and the glassy PS film will subsequently be floated on MilliporeTMwater and transferred from there onto a previously prepared PDMS-Si substrate. Chain length and dewetting temperature will be chosen such that the used PS can be considered as Newtonian liquid, e.g. with a molecular weight of 17 kg/mol, just below the entanglement length. Those polymers with high purity and small polydispersity index of typically $M_n/M_w \approx 1.04$ can be commercially purchased from e.g. Polymer Standard Services (PSS Mainz).

The dewetting process will be started by heating the sample above the glass transition temperature (T_g) of the PS film and will be monitored by optical microscopy (Zeiss Axiophot) on larger scales and by in-situ AFM (Bruker Icon with fast scan and heating option) on smaller scales. Using particular AFM imaging modes such as the HarmonixTM Nanoscale Material Property Mapping Mode (Bruker, Santa Barbara, USA) we aim at determining in parallel both the topography and the elasticity signals. A direct comparison of the topography and the complementary signals, fig. 5, allows to easily identify regions that correspond to undisturbed PDMS (green curve), regions with higher elasticity that corresponds to glassy PS (blue curve), and regions where the elastic modulus changes dramatically that corresponds to stretched PDMS ridges (red curve). Combining locally resolved topography with local material properties we expect to identify potential changes of surface tension via the adhesion force and potentially demixing of the elastomer. The latter might be expected for only partly cross linked and very soft elastomers. However, for substrates much softer than SG186 the Harmonix mode might not only be able to provide qualitative changes in elastic module. To obtain a tendency for demixing of the elastomer, we will additionally conduct bulk experiments determining the weight loss after leaching the non-cross linked molecules out of the elastomer using a good solvent. The deformation of the initially smooth elastomer interface that is caused by the dewetting PS will be determined by quenching the PS below its T_g , lifting the glassy PS dewetting structure off the substrate, and imaging the former liquid-elastomer interface by AFM. The lift-off technique works as follows: A drop of UV curable glue is poured on the sample and cured by UV light exposure. After curing, the solidified glue and with it the PS dewetting patterns where

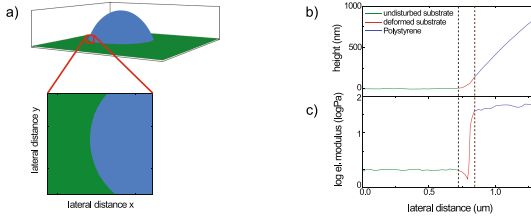


Figure 5: a) *Top*: 3d surface plot of an AFM scan of a PS droplet (blue) on a PDMS elastomer substrate (green) and (bottom) 2d zoom into the area of interest. Graphs of the cross-sections of the height b) and elasticity signal c).

the substrate deformation is frozen in are lifted off. We identify the particular PS feature on which we had earlier conducted the "top side" AFM measurement and image the same spot again. By combining the top and bottom side of the liquid morphology we "reconstruct" the 3d shape of the PS features on the PDMS substrate.

In preliminary experiments with SG184 and SG186 we achieved best results using the UV-curable pre-polymer "NOA 60". However, it needs to be checked that the chemical composition of this adhesive is compatible with the finally chosen elastomer materials to avoid undesired swelling of the elastomer substrate or migrating between the PS and the elastomer interface, which both can alter the structure that is imaged by AFM. The lift-off and imaging technique will be bench marked with equilibrium PS droplet shapes in comparison with literature results and with numerical results obtained within this tandem proposal and SPP collaboration partners. In that course we will also determine the static contact angle of the chosen systems by AFM. For very soft elastomers it will be important to check for potential "demixing" of a liquid part from a cross linked part upon dewetting and for a potentially strain dependent surface tension.

We estimate the time needed to optimize the PS film preparation, lift off and imaging protocols and to bench mark the 3d imaging protocol in total to 9 month.

WP E3: Explore Durotaxis (3 month) We also aim at exploring the possibility to study durotaxis on this experimental system. Depending on the exact system properties of the finally chosen elastomers it might be possible to observe "durotaxis" in the late stage of the dewetting process and individual droplets experience a force due to the strain field in the elastomer caused by surrounding neighbouring droplets. We will check if these effects appear by observing a completely dewetted sample (i.e. a pattern of droplets) for a extended period of time.

Additionally, we will try to prepare elastomer substrates with a gradient in elastic module or film thickness. A gradient of elastic module can potentially be obtained by gradients in cross linking densities that can be obtained for UV-curable elastomers such as Silopren 2030 (Momentive). Temperature gradient could be applied as well leading to different cross linking ratio. But it is expected that these different cross linking ratios will disappear quickly during dewetting as the dewetting temperature is well above the typical curing temperatures. This post-curing could only be avoided by poisoning the catalyst of the elastomer kid and will only be used if the other approaches fail. Thickness gradients can potentially be achieved when preparing elastomer films by squeezing them between a solid silicon support and an hydrophobized (e.g. Octadecyltrichlorosilane coated) glass or silicon substrate. It might be difficult to prepare a predefined thickness gradient, but it might be achievable to characterize the thickness gradients after preparation e.g. by AFM. Alternatively, it might be also possible to apply a homogeneous elastomer film thickness on top of a pre-structured solid substrate. Pre-structuring can be done by e.g. photolithographically obtained groove structures whose height is only a fraction of the elastomer thickness. It might even be enough to just offer on underlying photo-resist step to which the elastomer film adjusts

during spin-coating. If these type of sample preparation of "elastic gradients" is successful we aim at conducting dewetting experiments starting with thin PS films to obtain small PS droplets and observe their migration according to durotaxis. Durotaxis will depend on the system parameter and will be optimized to achieve a maximal interaction length within the available and developed PS-elastomer systems.

This work package is considered as explorative and meant to obtain a proof of concept within 3 month. When being successful we might continue it in collaboration with the project of Sebastian Aland and Uwe Thiele within this SPP and extend this project part in a potential second funding period.

WP E4: Dewetting Hole Growth Dynamics and Corresponding Characteristic Rim Shapes (15 month) The techniques and protocols developed in WP E1 and WP E2 will be applied to study the hole growth after rupture and the resulting rim shape. For these experiments we will use exclusively PS (presumably with molecular weights (10-18) kg/mol) that can be considered as a Newtonian liquid. The Newtonian behaviour will be confirmed by computing the Weissenberg number Wi by estimating the shear rate from the observed dewetting velocity. However for a potential second funding period also viscoelastic polymers might be considered.

Samples will be prepared following the protocol developed in WP E1 and WP E2. To start the dewetting, the temperature of the sample is raised from room temperature above T_g of the PS. The sample design (PS film thickness and elastomeric material) has to be optimized to follow the hole growth for long times and to potentially reach scale invariant rim profile shapes.

Due to its low T_g , the elastic module of the elastomeric films is less dependent on the temperature variations in the accessible range of $100^\circ C$ (T_g of PS) and $160^\circ C$ (PS scissoring) and will be mainly varied by cross-linking ratio or various elastomer types as identified in WP E1. Imaging by *in-situ* AFM will be done up to $135^\circ C$ using the fast scan head and up to $160^\circ C$ using the slower regular scan head.

As potentially occurring slip properties at the elastomer-liquid interface and the beginning of demixing of elastomer matrix and solvent is expected to be mainly visible in the early time behaviour, i.e. for very small hole radii, the hole growth dynamics shall be explored at small scales by *in situ* AFM imaging, see fig.1. For sufficiently slow hole growth dynamics locally material parameters shall be determined in parallel to the topography as described in WP E2. To obtain potential power laws the hole growth dynamics needs to be observed as long as possible, which will be done optically. For a precise matching of dewetting dynamics obtained by AFM and optical microscopy, a careful calibration of the different hot plates is mandatory. Provided the additional insight of local *in-situ* AFM measurements and the material properties are not needed, dewetting experiments can also be conducted at higher temperatures (in a protecting atmosphere) using optical microscopy while local topography, material parameters, and 3d rim shapes can be determined *ex-situ*. To obtain temporal/spatial development of rim shapes a series of dewetting experiments needs to be conducted with identical parameters as the sample is destroyed after each lift off process.

We aim at a comprehensive parameter study for both the rim dynamics and the rim shapes as function of different relative film thicknesses, PS viscosities and elastic module of the substrate film. The comparison with theoretical predictions shall be done by the parameter dependent hole growth dynamics and the emerging characteristic rim shapes using the experimentally determined system parameters such as film heights, viscosity and E-module as input values. Additional information will be provided by the (local) mechanical measurements that might shed light on potentially occurring demixing or strain dependent surface tension. By this comparison we aim at a detailed understanding of the underlying physical processes like strain dependent surface tension, potential demixing of the elastomeric material and in particular the energy dissipation during a moving three phase contact line.

The time needed to conduct complete time series including hole growth dynamics and rim shape evolutions for at least two different polymer viscosities, two elastomer films with different rheological properties, and two different film thickness ratios while keeping all other parameters fixed (this requires

at least four complete experimental data sets if parameters are chosen carefully) is estimated to about four month each, in total to about 15 months.

WP E5: Spinodal Dewetting of Newtonian fluids (2 month) We will also conduct tests to explore the spinodal dewetting of a liquid film on an elastomer substrate. This system will be extremely interesting but also challenging as two mobile interfaces will deform during this process. By quantitative comparison with theoretical results we expect to understand this process in depth, in particular also the mode selection process and the breakup dynamics. One particularly interesting feature of silicone-elastomers is that they are available with optical refractive indices ranging from about 1.4 to about 1.5 allowing to adjust the strength of the de-stabilizing van der Waals forces, e.g. [58]. To explore spinodal dewetting, we will use again for simplicity short chained PS that can be considered as Newtonian and one of the elastomers that was selected in the previous WP. The experimental challenge at the begin of the work task will be to prepare the right PS film thicknesses: Previous results from spinodal dewetting studies on solid substrates [37, 58] and a detailed analysis of the governing van der Waals forces suggest that a spinodal rupture process can be only observed in a very narrow parameter range. The spinodal break up time scales with h^5 and might be thus too fast for films thinner than about 3 nm and too slow for film thicknesses larger than about 8 nm where other rupture mechanism might be faster. However, because of the two mobile interfaces present in a liquid-elastomer dewetting system the observable regime of film height might be extended.

The sample preparation and the experimental procedure to explore the spinodal dewetting is very similar to what was explained in the previous WP and the emerging spinodal wavelength at the PS-air interface shall be imaged by fast *in situ* AFM scanning. The time evolution of the patterns will be analysed, e.g. by Fourier analysis, and compared to theoretical results. If required, a more detailed analysis of the topographic information using Minkowski measures will be applied, as previously done for spinodal dewetting pattern on solid substrates [37].

This last work package will only be started if time allows. For that reason it does not seem to be particularly useful to estimate a time for that but it seems unlikely to spend much more than **2 month** on that during the first funding period.

WP T1: Viscoelastic substrates, modelling and asymptotic reductions (15 months) The aim of this work package is concerned with the development of new continuum models for the dynamics of droplets and thin films on solid viscoelastic substrates. In some preliminary experiments R. Seemann and his group investigated the spreading of liquids in channels in elastic, soft substrates, i.e. silicon-rubber. They found that the spreading of the liquid filaments through the channels is surprisingly low and concluded that this is possibly related to earlier experimental and theoretical work by Carré and Shanahan [28] on the “braking” of running droplets on soft viscoelastic substrates. Due to the stress exerted on the solid at the contact line by the interfacial tension, the soft solid is locally raised and forms a “wetting ridge”. Upon passage of the contact line, the “wetting ridge” is released and so is some of the elastic energy, but not all. Since the solid is not perfectly elastic, a fraction of the energy is dissipated and this slows down the movement of the contact line. This energy dissipation can be much larger than the viscous dissipation in the liquid itself [28].

Our first goal will be the development of a continuum model and to derive corresponding lubrication models for the moving thin droplet as well as for a dewetting thin film. This will be used to systematically recover the wetting rates of spreading droplets on viscoelastic substrates. Another interesting and new problem is the impact of the viscoelastic layer on the dynamics, e.g. the dewetting rates, of a growing rim.

We will do this by using numerical simulations and complemented by analysis of the asymptotic structure of the droplet and the dewetting film by using matched asymptotics. From our experience

with dewetting films on solid and liquid substrates we assume that due to the different time scales on which the free surface and interfaces develop, there will be different asymptotic (time) regimes, where a characteristic dewetting rate can be identified.

Even for a simple system of a polymer droplet on a polymer brush, the density of the brushes induces wetting behaviour from complete wetting to dewetting. Moreover, the brush layer may also be deformable. For the case of dewetting films, the presence of a soft viscoelastic layer below the liquid generally destabilizes the film in that it increases the maximum growth rate of perturbations of a uniform film and the range of unstable wavelengths. It also leads to the formation of a characteristic “wetting ridge” in the solid where the growth of the perturbation leads to rupture of the liquid film. In order to develop a theoretical model for these processes, we treat the liquid layer $f(x, t) < z < h(x, t)$ as a Newtonian liquid, with a capillary surface at $z = h(x, t)$, resting on a viscoelastic substrate that extends from $z = -\ell$ to $z = f(x, t)$. We will formulate the model for this proposal only for the two-dimensional case, for simplicity. Then the equations governing the liquid are

$$\rho_l (\partial_t \mathbf{u}_l + \mathbf{u}_l \cdot \nabla \mathbf{u}_l) = -\nabla(p_l + \phi) + \mu_l \nabla^2 \mathbf{u}_l, \quad (6a)$$

$$\nabla \cdot \mathbf{u}_l = 0, \quad (6b)$$

where ρ_l is the density, $\mathbf{u}_l = (u, w)$ the velocity, with horizontal component u and vertical component w , p_l the pressure, and μ_l the viscosity in the liquid phase. The function ϕ represents the intermolecular forces, that we assume consists of one or more van-der-Waals term and a short range Born-repulsion type cut-off.

We start with a Kelvin-Voigt model for a homogeneous, isotropic incompressible viscoelastic medium

$$\sigma_s = -p_s \text{id} + G(\nabla \mathbf{u}_s + (\nabla \mathbf{u}_s)^T) + \mu_s \partial_t(\nabla \mathbf{u}_s + (\nabla \mathbf{u}_s)^T). \quad (7)$$

Plugging this into Newton’s second law and assuming incompressibility, yields the following governing equations for the solid bulk,

$$\rho_s \partial_{tt} \mathbf{u}_s = -\nabla p_s + G \nabla^2 \mathbf{u}_s + \mu_s \nabla^2 \partial_t \mathbf{u}_s, \quad (8a)$$

$$\nabla \cdot \mathbf{u}_s = 0, \quad (8b)$$

where ρ_s is the density, $\mathbf{u}_s = (s, r)$, with horizontal component s and vertical component r , denotes the displacement from the base state, p_s the pressure, G the shear modulus, and μ_s is the shear viscosity of the solid (i.e. viscoelastic) phase. At $z = -\ell$, we assume no-displacement boundary conditions,

$$\mathbf{u}_s = 0. \quad (9)$$

At the free surface of the liquid, we have the kinematic condition

$$\partial_t h + u \partial_x h = w. \quad (10)$$

and a force balance,

$$-\mathbf{n}_{out} \cdot \sigma_l + \sigma_{la} \frac{\partial_{xx} h}{(1 + (\partial_x h)^2)^{3/2}} \mathbf{n}_{out} = 0, \quad (11)$$

where σ_{la} denotes the liquid-air interfacial tension and

$$\mathbf{n}_{out} = \frac{(-\partial_x h, 1)}{(1 + (\partial_x h)^2)^{1/2}} \quad (12)$$

is the unit normal vector that points out of the liquid. The stress tensor in the liquid is given by

$$\sigma_l = -p_l \text{id} + \mu_l (\nabla \mathbf{u}_l + (\nabla \mathbf{u}_l)^T). \quad (13)$$

At the solid/liquid interface, $z = f(x, t)$, we have the kinematic conditions

$$\partial_t f + u \partial_x f = w, \quad (14)$$

and a force balance,

$$\mathbf{n}_{in} \cdot \sigma_l - \mathbf{n}_{in} \cdot \sigma_s + \partial_s (\Upsilon \mathbf{t}) = 0, \quad (15)$$

where Υ is the surface stress and

$$\mathbf{n}_{in} = \frac{(\partial_x f, -1)}{(1 + (\partial_x f)^2)^{1/2}}, \quad \mathbf{t} = \frac{(1, \partial_x f)}{(1 + (\partial_x f)^2)^{1/2}} \quad (16)$$

are the unit normal vector at the interface that points into the liquid and the tangent unit vector, respectively. Moreover, ∂_s is the tangential derivative. If the surface stress results from a constant liquid-solid surface energy σ_{sl} , so that $\Upsilon = \sigma_{sl}$, then we recover the usual mean curvature term in the force balance, that is,

$$\mathbf{n}_{in} \cdot \sigma_l - \mathbf{n}_{in} \cdot \sigma_s + \sigma_{sl} \kappa_s \mathbf{n}_{in} = 0, \quad (17)$$

with curvature

$$\kappa_s = \frac{\partial_{xx} f}{(1 + (\partial_x f)^2)^{3/2}}. \quad (18)$$

In general, we note, however, σ_{sl} is not constant for solids but depends on the surface strain due to the Shuttleworth effect [?], and if the surface strain is inhomogeneous along the interface, this give another, Marangoni-type term $(\partial_s \Upsilon) \mathbf{t}$ [7] on the left hand side of (17).

Finally, we assume impermeability of the solid,

$$(\partial_t \mathbf{u}_s - \mathbf{u}_l) \cdot \mathbf{n}_{in} = 0, \quad (19)$$

and a Navier-slip condition

$$(\partial_t \mathbf{u}_s - \mathbf{u}_l) \cdot \mathbf{t} = \frac{b}{\mu_l} \mathbf{n}_{in} \sigma_l \mathbf{t}, \quad (20)$$

since we are also interested in the case, where the liquid can slide past the solid.

Whenever possible will use asymptotic techniques to derive thin-film models from (6)–(14) and (17)–(20) for the moving thin droplet/film, and discuss asymptotically and numerically the long-time evolution of the dewetting process on viscoelastic substrates to obtain dewetting rates and large scale patterns for comparison to experimental results.

WP T2: Modelling soft polymer gels (8 months) For very soft polymer gels considered as networks of chemically or physically cross-linked polymer chains together with polymer chains moving through the network, we recently developed a new model that we will use to investigate the demixing or phenomena at the three-phase contact-line region.

The novelty of our approach here is to start with the modelling approach presented in [13], but include interfacial contributions to the free energy. We will use two coordinate system, one for the dry state of the gel, which we denote as the “initial” state, and one is the actual state. The transformation is described by the deformation gradient \mathbf{F} , and let $\det \mathbf{F}$. Variables and derivatives will be generally stated in the actual variables, unless otherwise stated or emphasized by the use of a subscript “0”. Thus, for example, \mathbf{j} and $\nabla \mu$ represent the flux vector and gradient operator in the actual configuration, while $\mathbf{j}_0 = J \mathbf{F}^{-1} \cdot \mathbf{j}$ and $\nabla_0 \mu = \nabla \mu \cdot \mathbf{F}$ is the corresponding notation for the initial state. In [13], Drozdov et al. allow for a separate reference state that represents the “as-prepared” gel; for simplicity, we assume here this is identical with the initial state, so we can use the two terms interchangeably. The variable C denotes the concentration of free polymer molecules (number of molecules per unit volume in the initial state), and

v the characteristic volume of a polymer molecule. The molecular incompressibility condition requires $J = 1 + Cv$.

Mass conservation and the equilibrium condition for the Cauchy stress are, respectively,

$$\dot{C} + \nabla_0 \cdot \mathbf{j}_0 = 0, \quad \nabla \cdot \mathbf{T} = 0. \quad (21)$$

The Helmholtz free energy (per unit volume in the initial configuration) has four contributions,

$$\psi = \psi_1 + \psi_2 + \psi_3 + \psi_4, \quad (22a)$$

with

$$\psi_1 = \mu_0 C, \quad \psi_2 = W(J_{e_1}, J_{e_2}, J_{e_3}), \quad \psi_3 = \frac{k_B T}{v \phi_n} (\phi_w \ln \phi_w + \chi \phi_w \phi_n), \quad \psi_4 = \frac{\eta(C)}{2} J \nabla C \cdot \nabla C. \quad (22b)$$

The first two contribution ψ_1 and ψ_2 are the energy of polymer molecules not interacting with the solid polymer network and the energy of the polymer network not interacting with polymer molecules, respectively, and ψ_3 is the energy of mixing of polymer molecules and segments of the polymer chains of the crosslinked network. The new contribution ψ_4 we add here is the interfacial energy between these two phases and at first assume an *ideal interface* [12]. Here J_{e_1} , J_{e_2} and J_{e_3} are the principal invariants of the Cauchy-Green tensor for elastic deformation, χ is the Flory-Huggins parameter, μ_0 denotes the chemical potential of a water molecule not interacting with the solid phase, k_B is Boltzmann's constant, T the absolute temperature, and $\eta(C)$ is constitutive expression controlling the magnitude of the interface energy between two phases. Phases in the gel are distinguished by a different composition, that is, different solvent concentrations. Also,

$$\phi_w = \frac{Cv}{1 + Cv}, \quad \phi_n = \frac{1}{1 + Cv}, \quad (23)$$

are the volume fraction of free polymer chains and cross-linked polymer network, respectively. For the strain energy density W , we adopt the neo-Hookean expression with shear modulus G ,

$$W = \frac{G}{2} [(J_{e_1} - 3) - \ln J_{e_3}]. \quad (24)$$

Transport of polymer molecules occurs through its diffusion through the polymer network, and we model this as

$$\mathbf{j} = -\frac{Dc}{k_B T} \nabla \mu, \quad (25)$$

where D is the diffusivity. Consistency with the energy imbalance inequality [13, 15] leads us to choose the following expressions for \mathbf{T} and μ , respectively, ($\mathbf{B} \equiv \mathbf{F} \cdot \mathbf{F}^T$),

$$\mathbf{T} = -\pi \mathbf{I} + \frac{2}{1 + Cv} \left[\frac{\partial W}{\partial J_{e_1}} \mathbf{B} - J_{e_3} \frac{\partial W}{\partial J_{e_2}} \mathbf{B}^{-1} - \left(J_{e_2} \frac{\partial W}{\partial J_{e_2}} + J_{e_3} \frac{\partial W}{\partial J_{e_3}} \right) \mathbf{I} + \frac{\partial \psi_4}{\partial \mathbf{F}} \right], \quad (26)$$

$$\mu = \mu_0 + k_B T \left[\ln \frac{Cv}{1 + Cv} + \frac{1}{1 + Cv} + \frac{\chi}{(1 + Cv)^2} + \frac{\Pi v}{k_B T} - \nabla \cdot (\eta(C) J \nabla C) \right]. \quad (27)$$

The osmotic pressure Π enters as the Lagrange parameter for the incompressibility condition. Inserting the expression for μ into (25) then gives an expression for the flux \mathbf{j} which has both Fickian ($\propto \nabla C$) and Darcy flow ($\propto \nabla \Pi$) contributions. Consistency of the latter with common expressions for Darcy flow then lead to

$$\mathbf{j} = -\frac{k_B T (1 + Cv)^{\beta-1}}{\zeta_0 v} \left[\frac{1 + (1 - 2\chi) Cv}{(1 + Cv)^3} \nabla C + \frac{Cv}{k_B T} \nabla \Pi + C \nabla \nabla \cdot (\eta(C) J \nabla C) \right], \quad (28)$$

where the last term results from the contribution of the interfacial energy, and where ζ_0 is a phenomenological constant and exponent $\beta = 1.5$. Upon transformation into initial state variables j_0 , this complements the mass conservation expression to determine the evolution of C .

The resulting model will be coupled to the equations for the liquid layer, with a nontrivial task to establish the appropriate interfacial and boundary conditions.

WP T3: Dynamics of droplet ensembles on soft substrates/gels (2 months) An interesting problem pursued by several groups within the SPP concerns the dynamics of droplet ensembles on soft substrates, in particular the problem of durotaxis. To understand the dynamics of large ensembles for long times we will explore a possible extension of the idea of asymptotic reduction of the model equations for the liquid droplets to a set of coupled ODE's taking into account only volume and location for each droplet. In Kitavtsev et al. [61] and [62] this idea was used to establish the long time dynamics of droplets interacting on a large scale. In the present case will be much harder as, due to the local deformations, the stress state of the substrate layer will nonlocally perturbed and effects the dynamics of other droplets.

WP T4: Numerical methods (7 months) In our group (at the WIAS) we have developed numerical algorithms to solve both the free boundary problems for Stokes' equations in various geometries via FEM, and corresponding thin-film models for a family of high-order thin-film PDE's, which we solve using spatially nonuniform finite differences and fully implicit Euler with adaptive time-stepping. In particular, we have applied our software to describe the evolution of the dewetting dynamics for a coupled liquid two-layer system including viscous and nonlinear viscoelastic rheologies, see e.g. [43], [48], [63]. We plan to extend the formulation and the numerical software first to the problem of linear elastic polymer layer.

Second, we also have developed numerical software for phase-field models of Cahn-Hilliard-type coupled to an elasticity equation using a linear model, in order to describe the phase separation and swelling behaviour during material infusion of the layer, see [59] and references therein. We will use this as a starting point for our numerical implementation of the two-layer system consisting of a liquid layer, or droplets on very soft elastomer. Most challenging and time consuming will be the extension of our formulation to the nonlinear elasticity model. Moreover, the numerical implementation needs to be extended in order to couple with the algorithm for the free boundary problem for Stokes' equations that governs the liquid flow.

WP T5: Spinodal dewetting (4 months) Once the new model(s), in particular the possible sharp-interface are established and validated through experimental comparison, we plan, as our first step to consider a thin liquid layer on top of a very soft substrate. The base states of this set up are constant but the mode selection and rupture process are challenging and on the level of complexity of the liquid-liquid rupture, that we have investigated before [49]. Moreover, any rupture event will perturb the stress state of the substrate globally. Already for the liquid two-layer system we have observed numerically self-similar approach towards rupture, and more complex, involving the lifting of the lower layer during the process. In particular for the polymer gel substrate, the question of finite/infinite time rupture, symmetry of the rupture solution are still not resolved, even though the literature on rupture phenomena for a single viscous layer or viscoelastic layer is much more developed but still not completely understood, see e.g. the recent discussions in [64].

2.4 Position of the project within the priority program

The reversible deformation of a elastomeric substrate close to a moving three phase contact line is a key to understand the energy dissipation, shape and dynamics of dewetting rims. We aim at developing mathematical models to predict dewetting dynamics of simple liquids from soft elastomeric to polymer

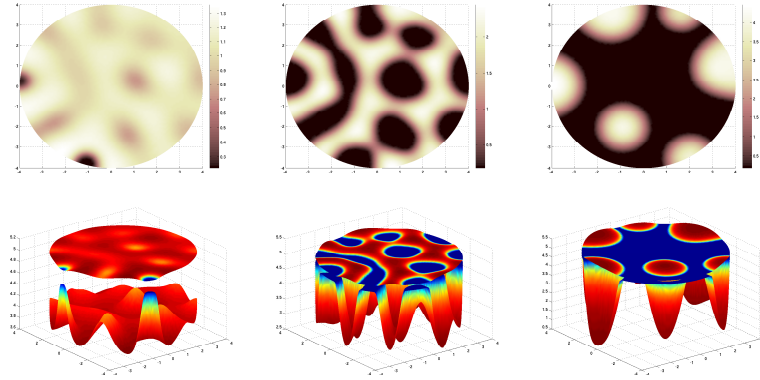


Figure 6: Spinodal decomposition in a liquid two layer system. Numerical simulations showing top and side view with initial layer thickness ratio 4 : 1 at three different times

gel substrates. A quantitative comparison with experimental results using the experimentally determined (locally resolved) material parameters shall allow for a detailed fundamental understanding of those processes and to confirm or to falsify certain effects that are discussed highly controversially in literature. This might be e.g. existence of the so called Shuttleworth effect for the considered experimental systems, potential separation of cross linked polymer network from non-cross linked molecules of the elastomer or any other effect that might explain the emerging depletion zone on the dry side of a dewetting ridge.

This topic is in the center of the priority program SPP2171, and several potential collaborations are already envisioned among other applying groups: We aim at comparing our results on equilibrium contact angle of liquid droplets on very soft elastomers with those from polyethylene glycol(PEG)-based hydrogels investigated in the project by Regine v. Klitzing, to better understand the underlying common properties. Also, regarding the dynamics, an in-depth understanding of the energy dissipation mechanisms coupling fluid flow with dissipative processes in the substrate is a major focus of the project by Dirk Peschka and will be central for many problems within this SPP, in particular we will discuss these issues for our models for the dewetting dynamics from soft elastomeric substrate. With the project by Axel Voigt we plan to compare his numerical diffuse-interface results with those obtained by sharp-interface models to be developed. Besides, we plan to explore durotaxis and shall compare to results from the project of Sebastian Aland as well as the project by Thiele/Snoeijer on the theory of ensembles of sitting and sliding droplets on elastic media. We will also discuss the possible effects of photo-switchable surface tension and wettability of the soft elastomer on the resulting (droplet) patterns together with the project by Holger Stark.

2.5 Data handling Theoretical and experimental data will be compared and analyzed and published in peer-reviewed international journals.

2.6 Other information NONE

2.7 Descriptions of proposed investigations involving experiments on humans, human materials or animals NONE

2.8 Information on scientific and financial involvement of international cooperation partners NONE

3 Bibliography

- [1] B. Andreotti, O. Bäumchen, et al., *Soft Matter*, 12(12):2993–2996, 2016.

- [2] R. Shuttleworth, *Proceedings of the Physical Society. Section A*, 63(5):444, 1950.
- [3] L. A. Lubbers, J. H. Weijs, et al., *Journal of Fluid Mechanics*, 747, 2014.
- [4] C.-Y. Hui, A. Jagota, *Soft Matter*, 11(46):8960–8967, 2015.
- [5] Q. Xu, R. W. Style, et al., *Soft Matter*, 14(6):916–920, 2018.
- [6] R. D. Schulman, M. Trejo, et al., *Nature Communications*, 9(1):982, 2018.
- [7] J. H. Snoeijer, E. Rolley, et al., *Physical Review Letters*, 121(6):068003, 2018.
- [8] P. J. Flory, J. Rehner, *The Journal of Chemical Physics*, 11(11):512–520, 1943.
- [9] M. A. Biot, *Journal of Applied Physics*, 26(2):182–185, 1955.
- [10] T. Tanaka, D. J. Fillmore, *The Journal of Chemical Physics*, 70(3):1214–1218, 1979.
- [11] T. Bertrand, J. Peixinho, et al., *Physical Review Applied*, 6(6), 2016.
- [12] W. Hong, X. Zhao, et al., *Journal of the Mechanics and Physics of Solids*, 56(5):1779–1793, 2008.
- [13] A. D. Drozdov, A. A. Papadimitriou, et al., *Mechanics of Materials*, 102:61–73, 2016.
- [14] S. A. Chester, L. Anand, *Journal of the Mechanics and Physics of Solids*, 58(11):1879–1906, 2010.
- [15] M. E. Gurtin, *Physica D: Nonlinear Phenomena*, 92(3):178–192, 1996.
- [16] K. E. Jensen, R. Sarfati, et al., *Proc. Nat. Acad. Sci.*, 112(47):14490–14494, 2015.
- [17] T. Salez, M. Benzaquen, et al., *Soft Matter*, 9:10699–10704, 2013.
- [18] R. B. J. W. R.W. Style, C. Hyland, E. R. Dufresne, *Nature Comm.*, 4(2728), 2013.
- [19] C.-Y. Hui, T. Liu, et al., 471(2175), 2015.
- [20] K. E. Jensen, R. Sarfati, et al., 112(47):14490–14494, 2015.
- [21] M. Ina, Z. Cao, et al., *ACS Macro Letters*, 6(8):854–858, 2017.
- [22] R. Pericet-Camara, A. Best, et al., *Langmuir*, 24(19):10565–10568, 2008.
- [23] B. Roman, J. Bico, *Journal of Physics: Condensed Matter*, 22(49):493101, 2010.
- [24] E. R. Jerison, Y. Xu, et al., *Phys. Rev. Lett.*, 106:186103, May 2011.
- [25] R. W. Style, Y. Che, et al., *Proc. Nat. Acad. Sci.*, 110(31):12541–12544, 2013. ISSN 0027-8424.
- [26] M. Rivetti, V. Bertin, et al., *Phys. Rev. Fluids*, 2:094001, Sep 2017.
- [27] M. E. R. Shanahan, A. Carre, *Langmuir*, 11(4):1396–1402, 1995.
- [28] M. E. R. Shanahan, *Journal of Physics D: Applied Physics*, 21(6):981, 1988.
- [29] A. Carré, M. E. Shanahan, *J. Coll. Int. Sci.*, 191(1):141 – 145, 1997. ISSN 0021-9797.
- [30] L. Chen, E. Bonaccurso, et al., *Langmuir*, 29(6):1893–1898, 2013.

- [31] A. Marchand, S. Das, et al., *Phys. Rev. Lett.*, 109:236101, Dec 2012.
- [32] J. B. Lee, S. dos Santos, et al., *Langmuir*, 32(32):8245–8254, 2016.
- [33] T. Kajiya, A. Daerr, et al., *Soft Matter*, 9:454–461, 2013.
- [34] T. Kajiya, P. Brunet, et al., *Soft Matter*, 10:8888–8895, 2014.
- [35] S. J. Park, B. M. Weon, et al., *Nature Comm.*, 5:4369, 2014.
- [36] R. Seemann, S. Herminghaus, et al., *Phys. Rev. Lett.*, 86(24):5534–5537, 2001.
- [37] J. Becker, G. Grün, et al., *Nature Materials*, 2:59–64, 2003.
- [38] R. Seemann, S. Herminghaus, et al., *Journal of Physics: Condensed Matter*, 17:267–290, 2005.
- [39] K. Jacobs, R. Seemann, et al., *Langmuir*, 14:4961–4963, 1998.
- [40] R. Seemann, S. Herminghaus, et al., *Phys. Rev. Lett.*, 87:196101, 2001.
- [41] R. Fetzer, K. Jacobs, et al., *Phys. Rev. Lett.*, 95:127801, 2005.
- [42] K. Kostourou, D. Peschka, et al., *Chem. Eng. Proc.: Process Intensification*, 50(5):531 – 536, 2011.
- [43] S. Bommer, F. Cartellier, et al., *Eur. Phys. J. E*, 36:13087, 2013.
- [44] D. Peschka, S. Bommer, et al., *Sci. Rep.*, 8:13295, 2018.
- [45] R. Seemann, M. Brinkmann, et al., *Journal of Physics: Condensed Matter*, 23(18):184108, 2011.
- [46] A. Carré, M. E. R. Shanahan, *Langmuir*, 17(10):2982–2985, 2001.
- [47] A. Carré, J.-C. Gastel, et al., *Nature Materials*, 379:432–434, 1996.
- [48] S. Jachalski, A. Münch, et al. Thin-film models for viscoelastic liquid bi-layers. WIAS preprint 2187
http://www.wias-berlin.de/preprint/2187/wias_preprints_2187.pdf.
- [49] S. Jachalski, A. Münch, et al., *J. Engin. Math.*, 86:9–29, 2014.
- [50] S. Jachalski, R. Huth, et al., *SIAM J. Appl. Math.*, 73(3):1183–1202, 2013.
- [51] P. Lambooy, K. Phelan, et al., *Phys. Rev. Lett.*, 76(7):1110, 1996.
- [52] A. Münch, B. Wagner, et al., *J. Engr. Math.*, 53:359–383, 2006.
- [53] C. Redon, F. Brochard-Wyart, et al., *Physical Review Letters*, 66(6):715–718, 1991.
- [54] J. Joanny, *Physicochemical Hydrodynamics*, 9(1-2):183–196, 1987.
- [55] M. Rauscher, R. Blossey, et al., *Langmuir*, 24:12290–12294, 2008.
- [56] R. Blossey, A. Münch, et al., *EPJ E - Soft Matter*, 20:267–27, 2006.
- [57] A. Münch, B. Wagner, et al., *EPJ E - Soft Matter*, 20:365–368, 2006.
- [58] R. Seemann, S. Herminghaus, et al., *Phys. Rev. Lett.*, 86(24):5534–5537, 2001.
- [59] E. Meca, A. Münch, et al., *Phys. Rev. E*, 97:012801, 2018.

- [60] A. Hemmerle, M. Schröter, et al., *Sci. Rep.*, 6:35650, 2016.
- [61] G. Kitavtsev, B. Wagner, *Journal of Engineering Mathematics*, 66(1):271–292, Mar 2010.
- [62] K. Glasner, T. Witelski, *Physica D: Nonlinear Phenomena*, 209(1):80 – 104, 2005.
- [63] S. Jachalski, D. Peschka, et al., *Trans. Proc. Fluid. Int.*, Adv. Math. Fluid Mech.:531–574, 2017.
- [64] A. A. Pahlavan, L. Cueto-Felgueroso, et al., *J. Fluid. Mech.*, 645:642–681, 2018.

4 Requested modules/funds

4.1 Basic Module

4.1.1 Funding for Staff

- a) For the experimental investigations we request funding of 75% TV-L-13 position at Saarland University.
- b) For the theoretical studies we request for a 75% E13 position to fund a doctoral student at the WIAS.

4.1.2 Direct Project Costs

Equipment up to Euro 10.000, Software and Consumables Saarland University: silicon wafer: Euro 400,- p.a.; AFM tips (regular tapping cantilever and 'fast scan' cantilever; imaging of liquid short chain polymers consumes many tips due to their stickiness: Euro 4500,- p.a.; cleavable mica sheets for the preparation process: EUR 200,- p.a.; ultraclean and monodisperse PS: Euro 300,- p.a; chemicals (organic solvents, acids for cleaning): Euro 600,- p.a. ; glass ware, tweezers, gloves: Euro 500,- p.a.. ; **Total EUR 6500 p.a..**

4.1.3 Travel Expenses

For visits national/international conferences and regular meetings with co-proposers of the priority program we request Euro 2500,- p.a. for travel and accommodation expenses per researcher at WIAS and Saarland University.

4.1.4 Visiting Researchers

Expenses for active participation in meetings Prof. Münch, Prof. Cook, Prof. Bertozzi (Euro 2000,- p.a)

4.1.5 Expenses for Laboratory Animals N.A.

4.1.6 Other Costs

4.1.7 Project-related publication expenses

WIAS Barbara Wagner asks to fund the publication of our findings either in form of articles, which will be submitted to leading, peer reviewed journals, partly with Open Access (1500 Euro/a).

Saarland University We apply for publication costs for journals like Phys. Rev. Lett, Sci. Reports, Nature Communications, New J. Phys. suitable for publishing combined theoretical and experimental results Euro 1500,- p.a.

4.1.8 Instrumentation

Major Instrumentation exceeding Euro 50,000 N.A.

Equipment exceeding Euro 10,000 To explore the dewetting of thin polymer films by optical microscopy a sensitive camera and a precisely controllable hot stage is needed allowing for good optical access and the possibility to flush the sample with protecting gas. Our available home build hot plate and temperature controller is meanwhile more than 15 years old and does not work reliably any more. We thus ask for a new hot stage including controller, such as the Linkam "LTS-420" (price EUR 13,200). Similarly, our available CCD camera (PCO pixelfly) cannot be upgraded for an up to date computer any more and runs only with Windows XP. Thus we also ask to upgrade this camera. For the planned experiment we need a sensitive color camera with at least 2000 pixel in one dimension and a frame rate of up to 30 fps. Color is requested to use the white light interference signal that helps to identify film thickness and profiles of dewetting rims. A camera that fulfills these requirements is e.g. "pco.edge 3.1" (price 13,000 EUR).

4.2 Module Temporary Position for Principle Investigator N.A.

4.3 Module Replacement Funding N.A.

4.4 Module Temporary Clinician Substitute N.A.

4.5 Module Mercator Fellows N.A.

4.6 Module Workshop Funding N.A.

4.7 Module Public Relations Funding N.A.

5 Project requirements

5.1 Employment status information

Ralf Seemann Professor at Saarland University (permanent) Prof. Dr. Barbara Wagner, has a permanent position at the WIAS and is (acting) head of the research group FG7 at the WIAS

5.2 First-time proposal data N.A.

5.3 Composition of the project group

Prof. Dr. Ralf Seemann, Postdocs: J.-B. Fleury, M. Brinkmann, M. Jung. Doct. student: W. Li, P. Shakeri, H. N. Tawfik, S. Puza, R. Shiri, N. Khangoli, L. Li, A.-L. Schuhmacher. Prof. Dr. Barbara Wagner, Postdocs: Dr. Rüdiger Müller, Dr. Clemens Guhlke, Dr. Manuel Landstorfer. Doct. student: Sibylle Bergmann

5.4 Cooperation with other researchers

5.4.1 Researchers with whom you have agreed to cooperate on this project

Prof. Dr. Regine von Klitzing (TU Darmstadt), Prof. Dr. Axel Voigt (TU Dresden). Dr. Sebastian Aland (Dresden), Dr. Dirk Peschka (WIAS), Dr. Martin Brinkmann (Saarland Univ.), Dr. Matthew Hennessy (Univ. Oxford), Prof. Dr. Andreas Münch (Univ. of Oxford), Prof. Dr. L. Pamela Cook (Univ. Delaware), Prof. Dr. Andrea Bertozzi (UCLA)

5.4.2 Researchers with whom you have collaborated scientifically within the past 3 years

Lou Kondic (NJIT), Shahriar Afkhami (NJIT), Ignacio Pagonabarraga (U-Barcelona), Vladimir Baulin (U Rovira I Virgili), Tak Shing Chan (U-Oslo), Joshua D. McGraw (ENS Research Univ.), Thomas

Salez (U-Bordeaux), Martin Brinkmann (U-Saarland), Ciro Semprebon (Northumbria Univ.), Stephan Herminghaus (MPI-DS, Göttingen), Oliver Bäumchen (MPI-DS, Göttingen), Gerhard Gompper (FZ-Jülich), Krishnacharya Khare (IIT-Kanpur), Bruce Law (Kansas State Univ.), Karin Jacobs (U-Saarland), Li-Jen Chen (Nat. Taiwan Univ.), Andreas Münch (U-Oxford), R. Blossey (Univ. Lille), Andrea Bertozzi (UCLA), Pam Cook (Univ. Delaware), John R. King (Univ. Nottingham), Ralf Blossey (U. Lille)

5.5 Scientific equipment

Saarland University AFM ICON (Bruker) with high temperature heater, fast scan upgrade and harmonix mode. Optical reflection microscope (Zeiss, Axiophot), equipped with high resolution camera and hot plate, ellipsometer (Optrel). Access to a Mars-2 rheometer to determine rheological bulk properties of the elastomers. Sample preparation: laminar flow bench, spin coater, ultrapure water supply, plasma cleaner, various drying oven, equipment to handle and degas PDMS mixtures.

WIAS Unix workstations and PC's, including software are available at WIAS.

5.5.1 Running costs for materials

WIAS will provide infrastructure, such as office space and general support i.e. secretary, seminar rooms. **Saarland University** provides the infrastructure such as office space, office supplies and office computer. About Euro 2000,- from the overall working group's general contribution can be spend per year for this project.

5.6 Project-relevant cooperation with commercial enterprises NONE

5.7 Project-relevant interests in commercial enterprises NONE

6 Additional information NONE